Pertanika J. Sci. & Technol. 34 (4): 2293 - 2310 (2026)

SCIENCE & TECHNOLOGY

Journal homepage: http://www.pertanika.upm.edu.my/

Partial Discharge Detection and Localisation in Refined, Bleached and Deodorised Palm Olein Based on Ultra-High Frequency Sensing Technique

Nur Darina Ahmad[1,2], Norhafiz Azis[1]*, Zhi Yang Lim[1], Jasronita Jasni[1], Khairil Anas Md Rezali[3], Mohd Aizam Talib[4], Nik Hakimi Nik Ali[5], and Masahiro Kozako[6]

[1]*Advanced Lightning, Power and Energy Research Centre (ALPER), Faculty of Engineering, Universiti Putra Malaysia, 43400 UPM Serdang, Selangor, Malaysia*
[2]*Electrical Engineering Studies, Universiti Teknologi MARA Cawangan Pulau Pinang, Permatang Pauh Campus, 13500 Seberang Perai, Pulau Pinang, Malaysia*
[3]*Department of Mechanical and Manufacturing Engineering, Faculty of Engineering, Universiti Putra Malaysia, 43400 UPM Serdang, Selangor, Malaysia*
[4]*Advanced Diagnostic Services, TNB Labs Sdn. Bhd., 43000 Kajang, Selangor, Malaysia*
[5]*School of Electrical Engineering, College of Engineering, Universiti Teknologi MARA (UiTM), 40450 Shah Alam, Selangor, Malaysia*
[6]*Department of Electrical and Electronic Engineering, Kyushu Institute of Technology, 804-8550 Kitakyushu-shi, Fukuoka, Japan*

ABSTRACT

This study presents a comparative analysis of Partial Discharge (PD) detection and localisation in Mineral Oil (MO) and Refined, Bleached and Deodorised Palm Olein (RBDPO) based on the Ultra-High Frequency (UHF) technique. A PD experiment was arranged using a needle–plane electrode configuration, and the gap was set to 35 mm. To initiate the PD, the applied voltage was gradually increased from 15 kV to 25 kV in 5 kV/step. In total, 4 patch-type UHF sensors were mounted externally on the steel tank wall at predetermined locations to capture the PD signals. An electrical PD event was detected simultaneously using an Impedance Matching Circuit (IMC). The UHF PD signals were denoised by a Gaussian filtering method. The Time Difference of Arrival (TDOA) was then determined through the First Peak Method (FPM) and Cumulative Energy Method (CEM). PD localisation was carried out based on the TDOAs obtained from both FPM and CEM. It is found that although RBDPO exhibits higher attenuation of UHF PD signals, it achieves lower

ARTICLE INFO

Article history:
Received: 19 March 2026
Accepted: 05 August 2026
Published: 20 August 2026

DOI: https://doi.org/10.47836/pjst.34.4.16

E-mail addresses:
nurdarina9183@uitm.edu.my (Nur Darina Ahmad)
norhafiz@upm.edu.my (Norhafiz Azis)
gs68246@student.upm.edu.my (Zhi Yang Lim)
jas@upm.edu.my (Jasronita Jasni)
khairilanas@upm.edu.my (Khairil Anas Md Rezali)
aizam.talib@tnb.com.my (Mohd Aizam Talib)
hakimiali@uitm.edu.my (Nik Hakimi Nik Ali)
kozako@ele.kyutech.ac.jp (Kozako Masahiro)
* Corresponding author

e-ISSN: 2231-8526

localisation error as compared to MO. Performance assessment further confirms that PD localisation is better in RBDPO than in MO.

Keywords: Cumulative energy method, first peak method, partial discharge localisation, refined, bleached and deodorised palm olein, ultra-high frequency

INTRODUCTION

Partial Discharge (PD) is an electrical occurrence that happens within insulating materials that are subjected to high voltage stress. It is well acknowledged as a preliminary sign of insulation deterioration in high-voltage apparatus such as power transformers. If PD is left unaddressed, it can cause insulation failure, dielectric breakdown, unexpected power outage and costly repair or replacement of the equipment (Chan et al., 2023; Rathod et al., 2021; Thiviyanathan et al., 2022). Therefore, comprehensive detection and localisation of PD are essential for condition-based monitoring and preventative maintenance in electricity systems (Duan et al., 2019).

Mineral Oil (MO) has been the primary insulation and cooling agent in transformers since its inception. However, the extensive use of fossil-based products has raised concerns over environmental pollution and sustainability (Adak & Cangi, 2024). Consequently, researchers have investigated biodegradable dielectric insulating fluids as alternatives to MO. Researchers in (Muangpratoom et al., 2023) examined the electrical and physicochemical properties of various batches of palm oil. The efficacy of acoustic emission-based PD detection in soybean oil was evaluated by Qian et al. (2018). Mohamad et al. (2021) examined the impact of aluminium oxide nanoparticles on the PD properties of palm oil and coconut oil. Meanwhile, Mina-Casaran et al. (2025) and Mohan Rao et al. (2019) examined rapeseed oil and sunflower oil that can be used as alternatives to MO. Among the various potential alternatives, Refined, Bleached and Deodorised Palm Olein (RBDPO) has garnered considerable interest due to its beneficial dielectric and thermal properties. In addition, high biodegradability, low toxicity and wide availability in Southeast Asian countries made RBDPO a more attractive choice as a sustainable dielectric insulating fluid for transformers (Ahmad et al., 2025; Azis et al., 2014; Azmi et al., 2017; Girish et al., 2021; Mina-Casaran et al., 2025; Mohamad et al., 2014).

PD is a rapid electrical phenomenon that produces electromagnetic waves within the Ultra-High Frequency (UHF) band. The UHF sensing technique is widely applied to detect and locate PDs in transformers. It offers a higher Signal-to-Noise Ratio (SNR), better sensitivity and stronger immunity to electromagnetic interference than the conventional electrical PD method (Antony et al., 2021; Chai et al., 2019; Desai & Sarathi, 2018; Jangjoo et al., 2023; Uwiringiyimana et al., 2022). The principle of the technique relies on the detection of electromagnetic signals between 300 MHz and 3 GHz through UHF sensors (Gautam et al., 2023; Gautam et al.,2024).

The UHF PD localisation critically depends on the Time Difference of Arrival (TDOA) computation. The First Peak Method (FPM) and the Cumulative Energy Method (CEM) are commonly used to determine the TDOA based on the PDs. For FPM, the PD signal is converted to unipolar form and normalised to a common amplitude scale. The earliest peak that exceeds a pre-defined threshold is taken as the Time of Arrival (TOA) of the PD signal. This method is less affected by multipath reflections and often provides good output for TDOA computation (Ha et al., 2018; Song, 2004). On the other hand, CEM identifies the TDOA based on the Cumulative Energy (CE) curve of the PD signal. It is suitable for noisy environments and for PD signals with low SNR, as the CE profile is less affected by the instantaneous fluctuations in signal amplitude (Sinaga et al., 2011; Xavier et al., 2021).

Currently, research on PD phenomena in natural esters, such as RBDPO, remains at an early stage (Gautam et al., 2023; Gautam et al., 2024). Previous studies have mainly focused on the investigation of PD characteristics and detection in natural esters, while studies that are related to UHF PD localisation are still limited (Lam, 2024; Mengounou et al., 2022; Rajab et al., 2025). Therefore, this study aims to experimentally investigate the feasibility of UHF PD localisation in RBDPO. An experiment is established to generate PD in a test tank by means of a needle-plane electrode configuration. The UHF PD signals are acquired through 4 patch-type UHF sensors mounted on the external surface of the tank wall. In addition, an Impedance Matching Circuit (IMC) is employed to record the electrical PD signals and verify the PD occurrence. The UHF PD signals are denoised by a Gaussian filter, and the FPM and CEM are applied to determine the TDOA from the denoised PD signals. Finally, the PD localisation in either MO or RBDPO is carried out based on the calculated TDOAs and a non-iterative algorithm that locates the PD location without iterative optimisation, thus reducing computational time. The main contribution of this study is the experimental validation of UHF PD localisation in RBDPO and its quantitative comparison with conventional MO under controlled experimental conditions.

METHODOLOGY

Oil Sample Preparation

RBDPO served as the test sample in this study, while MO was employed for comparison. The properties of the MO and RBDPO used in this study are listed in Table 1 (Dombek & Gielniak, 2023; Mohamad et al., 2018). The preparation of the oil samples involved filtration and drying to ensure that the oil samples were clean and to reduce the moisture content. Filter paper with a 0.22 µm pore size was utilised to filter the oil samples. The drying process was conducted at 85 °C for 48 hours for MO and 72 hours for RBDPO. After drying, the moisture contents of the MO and RBDPO were 12 ppm and 109 ppm, respectively. In total, 65 litres of MO and 65 litres of RBDPO were filtered, dried, and filled into the test tank for the PD test.

PD Experiment Setup

Table 1
Oil properties

Properties	Unit	MO	RBDPO
Density at 20 °C	kg/dm^3	0.88	0.89
Viscosity at 40 °C	cSt	8.7	37.3
Permittivity	-	2.19	2.78
Breakdown Voltage (2.5 mm gap, after treatment)	kV	55	52

The PD experiment setup was conducted according to the IEC 60270 standard, as shown in Figure 1 (Ahmad et al., 2023). A needle-plane electrode pair was employed to generate ionisation (Murad et al., 2025), with the gap between the needle tip and the plane electrode fixed at 35 mm. The strong electric field produced at the needle tip enabled stable and repeatable PD generation. Therefore, this defect model is commonly adopted in PD localisation experiments (Wu et al., 2022). The dimensions of the steel test tank were 100 cm in length, 30 cm in width, and 25 cm in height, and it was grounded. The lower-left corner at the back of the test tank was taken as the origin of the tank's coordinate system. The x-, y-, and z-axis orientations are illustrated in Figure 2. Based on this coordinate system, the PD source was placed at the coordinates 0.50 m, 0.08 m, 0.15 m inside the tank. The temperature in the experimental environment ranged from 26 °C to 28 °C, while the relative humidity ranged from 53% to 69%. In total, 10 different sensor configurations were employed for UHF PD signal acquisition, and the coordinates of the 4 UHF sensors for each of the configurations are listed in Table 2. For both MO and RBDPO, 3 UHF PD measurements were taken for each of the sensor configurations.

For PD detection, 4 commercially available patch-type UHF sensors with an operating frequency range from 0.7 GHz to 2.7 GHz were used. The specifications of the UHF sensors are outlined in Table 3. The UHF PD signals were recorded by a LeCroy WaveMaster

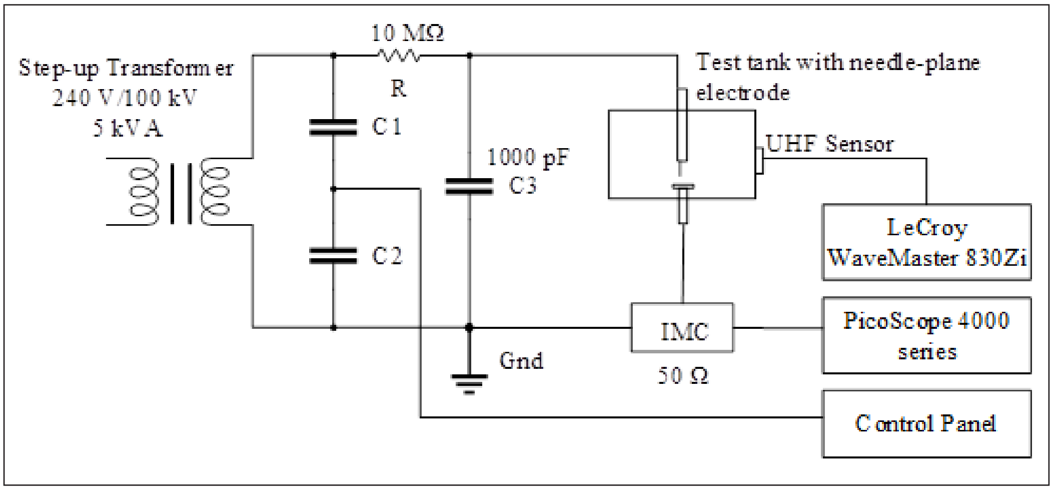

Figure 1. Schematic diagram of PD experiment using UHF sensor configuration

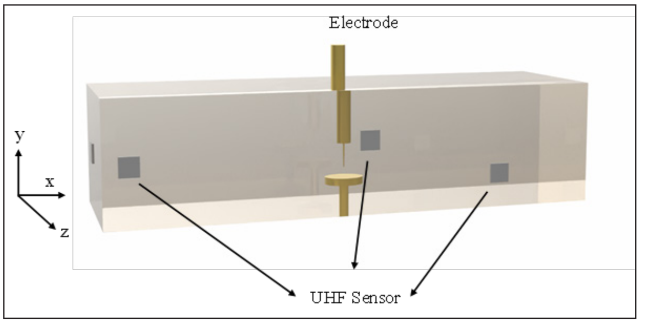

Figure 2. Electrode and sensor placement

Table 2
Coordinates of the 4 UHF sensors for the 10 experimental configurations

Sensor Configuration	Sensor 1 (x, y, z) (m)	Sensor 2 (x, y, z) (m)	Sensor 3 (x, y, z) (m)	Sensor 4 (x, y, z) (m)
1	1.00, 0.15, 0.15	0.75, 0.15, 0.30	0.10, 0.05, 0.30	0.00, 0.10, 0.20
2	1.00, 0.15, 0.15	0.60, 0.10, 0.30	0.35, 0.10, 0.30	0.00, 0.10, 0.20
3	1.00, 0.10, 0.10	0.80, 0.05, 0.30	0.45, 0.05, 0.30	0.95, 0.15, 0.00
4	1.00, 0.05, 0.25	0.20, 0.15, 0.30	0.70, 0.05, 0.30	0.90, 0.15, 0.00
5	0.10, 0.15, 0.00	0.20, 0.15, 0.30	0.60, 0.10, 0.30	0.95, 0.10, 0.00
6	0.10, 0.15, 0.00	0.20, 0.15, 0.30	0.85, 0.10, 0.30	0.95, 0.05, 0.00
7	0.05, 0.15, 0.00	0.10, 0.15, 0.30	0.45, 0.15, 0.30	1.00, 0.05, 0.15
8	0.05, 0.15, 0.00	0.10, 0.15, 0.30	0.50, 0.10, 0.30	0.85, 0.15, 0.00
9	0.00, 0.15, 0.15	0.20, 0.10, 0.30	0.45, 0.15, 0.30	1.00, 0.05, 0.15
10	0.00, 0.15, 0.15	0.20, 0.10, 0.30	0.70, 0.15, 0.30	0.90, 0.10, 0.00

830Zi oscilloscope operated at a sampling rate of 40 GS/s and a bandwidth of 3 GHz to ensure high-resolution data collection. Meanwhile, an electrical PD signal was acquired to verify the occurrence of PD. The electrical PD signals were measured through an IMC and recorded by a PicoScope 4824 oscilloscope at a sampling rate of 80 MS/s and a bandwidth of 20 MHz. The calibration of the IMC was performed with a JZF-10 external calibrator to establish the voltage level that corresponded to an apparent charge of 100 pC (Working Group D1.33, 2012). Only UHF signals that occurred simultaneously with an IMC voltage above the calibrated threshold were considered as valid PD signals.

Table 3
UHF sensor specifications

Parameter	Specification
Return Loss	-9 dB
Efficiency	45%
Peak Gain	2 dBi
Average Gain	-3.5 dB
Radiation Pattern	Omni-directional

PD Signal Denoising and TDOA Computation

The UHF PD signals were denoised by Gaussian filtering before the TDOA determination process (Šefl et al., 2023). The employed Gaussian filter consisted of a Gaussian kernel derived from the Gaussian distribution, as expressed in Equation 1.

$$G(x) = \frac{1}{\sqrt{2\pi\sigma^2}} e^{-\frac{x^2}{2\sigma^2}} \quad [1]$$

In this equation, σ denotes the standard deviation that controls the width of the filter, and x is the distance from the kernel centre. In this study, σ was set to 10. Noise reduction was performed through a convolution between the UHF PD signal and a Gaussian kernel, as given in Equation 2.

$$S_{denoised}\,(n) = \int_{-\infty}^{\infty} S_{raw}\,(t) G(n-t)\, dt \quad [2]$$

In Equation 2, n represents the data point of the denoised UHF PD signal, whereas t denotes the data point in the raw UHF PD signal. $S_{raw}\,(t)$ and $S_{denoised}\,(n)$ are the raw and denoised UHF PD signals, respectively.

The FPM and CEM were subsequently used to compute the TDOA from the denoised UHF PD signals. In the FPM, the denoised UHF PD signals were subjected to unipolar conversion to ensure consistency in polarity while the amplitude characteristics of the PD signals were preserved. This conversion reduced the effects of phase shift and waveform distortion and allowed for reliable comparisons of PD signals from different sensors. The UHF PD signals were then normalised to a uniform amplitude range between 0 and 1. This step was necessary to ensure comparable amplitude levels among the PD signals, especially in RBDPO, where attenuation was apparent. The TOA for each of the UHF PD signals was determined as the time of the first local peak that exceeded an amplitude threshold of 0.25. Sensor 1 was designated as the reference sensor, and the TDOAs were computed as the difference between the TOA at the reference sensor and the TOAs at the other three sensors.

For CEM, the CE curve of each of the UHF PD signals was first calculated based on Equation 3.

$$U_k[n] = \sum_{n=1}^{N} x_k^2[n] \quad [3]$$

In Equation 3, U_k represents the CE curve, x_k denotes the UHF PD signal from the sensor k, and N is the total number of data points in the UHF PD signal. The similarity function in Equation 4 was then applied to determine the TDOAs between the reference sensor and the other three sensors.

$$S[t_l] = \sum_{i=1}^{N-l} |U_1(t_i) - U_k(t_{i+l})|; \quad k = 2, 3, 4 \qquad [4]$$

In this equation, U_1 and U_k are the CE curves from the reference sensor and the kth sensor, respectively, and l denotes the amount of time shift between the two curves. Since the UHF PD signals were sampled at 40 GS/s, one unit difference in l corresponded to a time interval of 25 ps. The time shift l that produced the lowest value of $S[t_l]$ was taken as the TDOA between the reference sensor and the kth sensor (Sinaga et al., 2012).

PD Localisation Based on TDOA

The non-iterative algorithm in (Sinaga et al., 2012) was employed to perform PD localisation based on Equations 5 and 6.

$$\begin{bmatrix} x \\ y \\ z \end{bmatrix} = -[x_{mn} \quad y_{mn} \quad z_{mn}]^{-1} \times \left[(r_{mn}) r_n + \frac{1}{2} ({r_{mn}}^2 - K_m + K_n) \right] \qquad [5]$$

$$r_n^2 = (x - x_n)^2 + (y - y_n)^2 + (z - z_n)^2 \qquad [6]$$

In Equation 5, n denotes UHF sensor 1, which serves as the reference sensor, while m corresponds to UHF sensors 2, 3, and 4. The term r_{mn} represents the TDOA between sensor m and sensor n, multiplied by the propagation velocity of the UHF PD signal in the insulation medium under consideration. The unknown term r_n indicates the distance from the reference sensor to the PD source, and K_m and K_n are defined as $K_j = x_j^2 + y_j^2 + z_j^2$. The TDOAs derived from the FPM and CEM were used in Equation 5 to express the PD source coordinates, (x, y, z) in terms of r_n. The quadratic equation in Equation 6 was then solved to obtain 2 roots, which were substituted back into Equation 5 to compute the PD source location.

Equation 7 was employed to compute the propagation velocity of the UHF PD signal either in RBDPO or MO. In this equation, v denotes the propagation velocity of the UHF signal in the insulation medium, s_l refers to the speed of light in a vacuum, and ε_r represents the relative permittivity of the insulating liquid. In this study, s_l was taken as 3×10^8 m/s and ε_r was set to 2.78 for RBDPO. Under these conditions, the calculated velocity of the

UHF PD signal in RBDPO was 1.7992 × 10^8 m/s (Mohamad et al., 2014). Similarly, the propagation velocity of the UHF PD signal in MO was computed as 2 ×10^8 m/s. Since the UHF PD signals were sampled at 40 GS/s, the oscilloscope provided a temporal resolution of 25 ps. This corresponded to a spatial resolution of approximately 5 mm in MO and 4.5 mm in RBDPO for the TDOA-based PD localisation method.

$$v = \frac{s_l}{\sqrt{\varepsilon_r}} \quad [7]$$

The accuracy of UHF PD localisation in both MO and RBDPO was evaluated through the localisation error (LE) and relative error (RE) as defined in Equations 8 and 9 (Mohd Hashim et al., 2022).

$$LE = \sqrt{\left(x_{actual} - x_{computed}\right)^2 + \left(y_{actual} - y_{computed}\right)^2 + \left(z_{actual} - z_{computed}\right)^2} \quad [8]$$

$$RE = \frac{LE}{Tank\ Diagonal} \times 100 \quad [9]$$

The Mean Squared Error (MSE) and Root Mean Squared Error (RMSE) were also employed to assess the PD localisation accuracy along the x-, y- and z-axes (Perfetto and D'Antona, 2021; Khodaveisi et al. 2024). These metrics measure the deviation between the estimated and actual PD coordinates. Lower MSE and RMSE indicate high PD localisation accuracy.

RESULTS AND DISCUSSION

Amplitude of UHF PD Signals in MO and RBDPO

The average, maximum, and minimum amplitudes of the UHF PD signals in MO and RBDPO are presented in Figure 3. The amplitudes of the UHF PD signals are generally higher in MO than in RBDPO. This is possibly due to differences in the dielectric loss properties of the 2 oil samples (Dombek & Gielniak, 2023). The percentage difference in average amplitude between MO and RBDPO is 92.7%. For the maximum and minimum amplitudes, the percentage differences are 92.4% and 91.3%, respectively.

Denoising of UHF PD Signals in MO and RBDPO

Figure 4 shows an instance of the raw and denoised UHF PD signals in MO. It is found that the raw UHF PD signal exhibits a distinct peak at the start of the discharge event, and

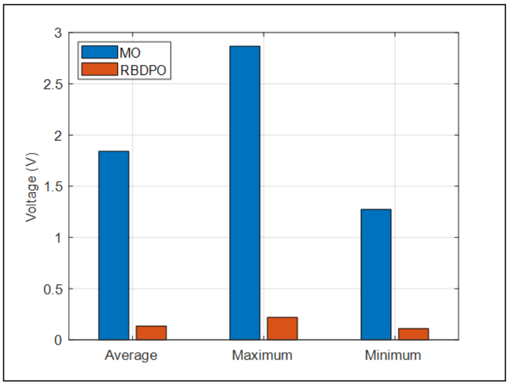

Figure 3. Amplitudes of the UHF PD signals in MO and RBDPO

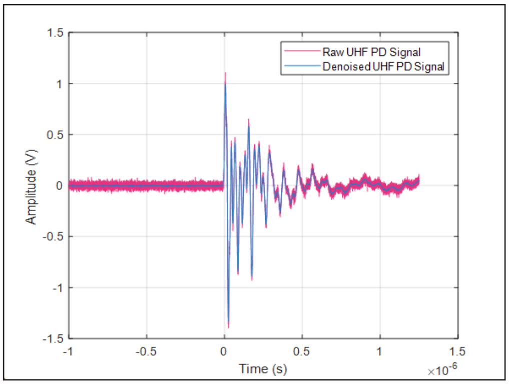

Figure 4. Raw and denoised UHF PD signals in MO

it is followed by oscillations that gradually decay over time. The amplitude reaches ± 1.1 V, which suggests a less obstructed propagation path in MO as compared to RBDPO. A moderate level of background noise appears before and after the main PD events, which is anticipated due to the electromagnetic interference. The UHF PD signal denoised by the Gaussian filter preserves the main waveform structure, while the background noise is largely reduced.

Figure 5 shows the raw and denoised UHF PD signals in RBDPO. The raw UHF PD signal has a similar structure to that in MO, which consists of an initial peak, and it is followed by damped oscillations. However, the amplitude is relatively low, at ± 0.09 V, which indicates that RBDPO exhibits stronger attenuation characteristics than MO. The background noise in RBDPO appears slightly higher than in MO, possibly due to the differences in dielectric properties, such as its viscosity, permittivity, and conductivity, which may affect the propagation and dispersion of UHF PD signals (Chandrasekar & Montanari, 2014; Jaroszewski & Rakowiecki, 2017; Khelifa et al., 2024). The denoised UHF PD signal shows a significant improvement in clarity, whereby the background noise is reduced by 79.9%. Nevertheless, the overall amplitude remains lower than in MO, which peaks at ± 0.08 V. The oscillations after the initial PD event become more distinct in the denoised UHF PD signal, which may facilitate the PD localisation analysis.

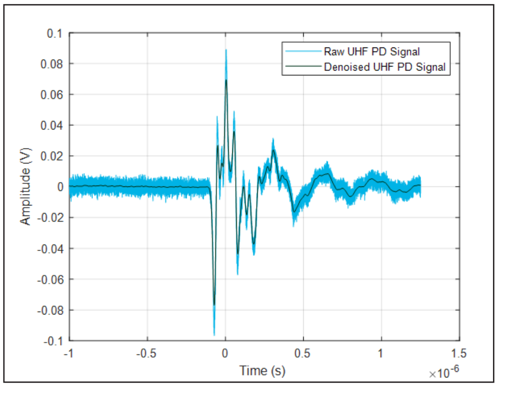

Figure 5. Raw and denoised UHF PD signals in RBDPO

TDOA Determination

First Peak Method

The UHF PD waveforms in MO and RBDPO after unipolar conversion and normalisation are illustrated in Figures 6(a) and 6(b). A 0.25 amplitude threshold is applied in the FPM to ensure that the TOA is identified from the actual first peak of the UHF PD signals instead of the background noise. For MO, the normalised waveforms exhibit several early peaks with amplitudes up to 0.99 p.u., and slowly decay, as depicted in Figure 6(a). The normalised UHF PD signals in RBDPO show sharp initial peaks with amplitudes up to 0.99 p.u., which lead to attenuated peaks. It is found that after the initial peaks, the amplitudes of the UHF PD signal in RBDPO are lower than those in MO. The UHF PD waveforms in RBDPO are more damped, as indicated by the fewer oscillations after 0.5 μs, as in Figure 6(b). These PD waveform characteristics suggest a higher dielectric loss and a relatively obstructed propagation medium for UHF signals in RBDPO. Although the PD signal duration is shorter in RBDPO, the relatively clearer initial peaks likely improve the localisation accuracy. These observations agree with previous studies on the impact of oil properties on UHF signal behaviour and PD detection in RBDPO (HadiAlnashia et al., 2018; Muangpratoom et al., 2023; Suhaimi et al., 2025).

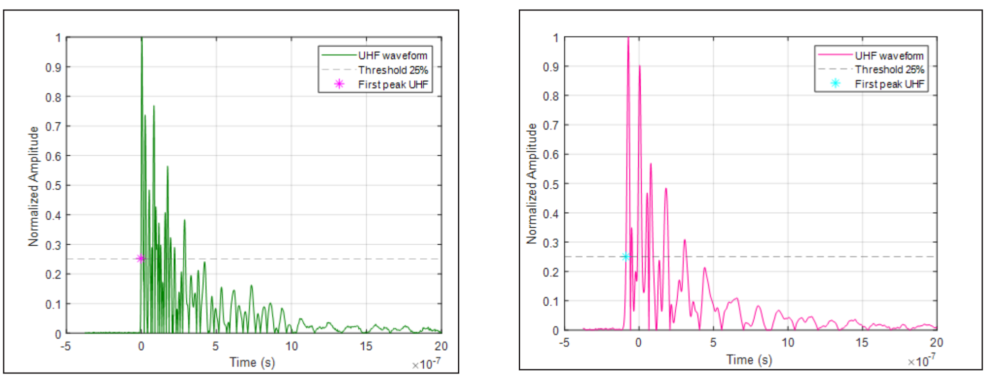

(a) (b)

Figure 6. UHF PD signals in (a) MO and (b) RBDPO after unipolar conversion and normalisation in the FPM

Cumulative Energy Method

The CE curves of the UHF PD signals in MO and RBDPO are depicted in Figures 7(a) and 7(b). The UHF PD signals in both MO and RBDPO show similar CE patterns, where the curves start with a flat region and increase rapidly, marking the occurrence of the PD event. In MO, the CE curve exhibits a steep and abrupt transition across all sensors. As seen in Figure 7(a), the normalised CE curve rises abruptly from zero to unity within a narrow time range of less than 1 ns. This sharp transition indicates strong PD signal intensity and stable propagation of the UHF PD signal through MO. In contrast, the CE curve of the UHF PD signals in RBDPO displays a more gradual rise, and the overall slope is lower than that of MO, as illustrated in Figure 7(b). This can be attributed to the higher permittivity and viscosity of RBDPO, which tend to attenuate and slow down UHF wave propagation in the medium (Durga et al., 2020; Kurimský et al., 2021). For both MO and RBDPO, the CE curves from each of the sensors are closely aligned; hence, the TDOAs between the collected UHF PD signals fall within the nanosecond range.

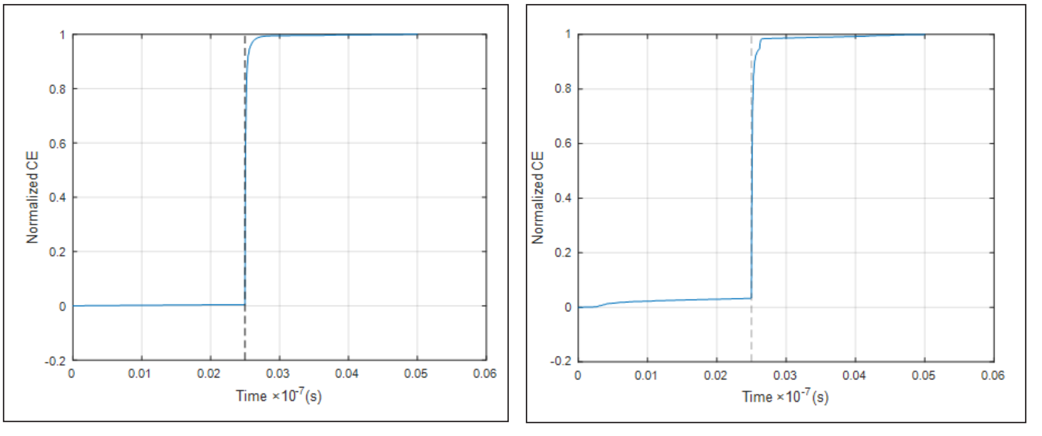

(a) (b)

Figure 7. Normalised CE curves of UHF PD signals in (a) MO and (b) RBDPO

PD Localisation

The LE and RE for PD localisation in MO and RBDPO are shown in Figure 8. Each data point represents the average of the 30 UHF PD measurements. For TDOAs from the FPM, the PD localisation in RBDPO is better than in MO, where the LE in MO is 2.27 cm higher than in RBDPO. This is consistent with the RE, as the RE of PD localisation in RBDPO is 2.1% lower than in MO. In contrast, the PD localisation in MO is better than in RBDPO for TDOAs from the CEM, where the LEs are 54.22 cm and 56.83 cm, respectively. Similarly, the RE of PD localisation in MO is 2.4% lower than in RBDPO. The standard deviations of the PD LEs are also presented in Figure 8. For the FPM, the standard deviations of the LEs in MO and RBDPO are 18.24 cm and 17.23 cm, whereas for the CEM, the standard deviations are 17.73 cm and 17.55 cm for RBDPO and MO, respectively. The comparable standard deviations among the 4 cases suggest that the spread of the PD LEs is similar under different types of oil samples and TDOA estimation methods. Overall, the TDOAs from the FPM produce lower LE than those obtained from CEM. Furthermore, for TDOAs from the FPM, PD localisation in RBDPO results in lower LE than in MO. The higher PD localisation accuracy in RBDPO is likely due to its higher permittivity as compared to MO, which could help to reduce multipath reflections and improve the SNR of UHF PD signals (Azis et al., 2014; Mu et al., 2024; Yu & Zhang, 2024). Although the theoretical spatial resolution for PD localisation is approximately 5 mm in MO and 4.5 mm in RBDPO, the experimental PD LEs are considerably larger. This is because the practical PD localisation accuracy depends not only on the temporal resolution of the PD detection system but also on measurement noise, multipath propagation, and error in TDOA estimation.

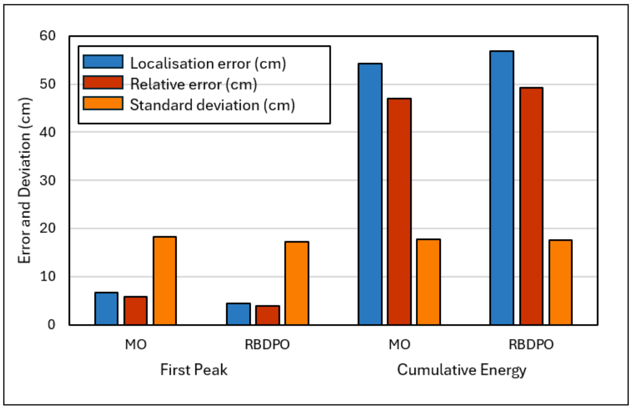

Figure 8. Localisation error (LE) and relative error (RE) of PD localisation in MO and RBDPO based on TDOAs obtained from FPM and CEM

Table 4
MSE and RMSE of PD localisation based on TDOAs from the FPM

	MO			**RBDPO**		
	X	**Y**	**Z**	**X**	**Y**	**Z**
MSE (mm^2)	0.42	12.91	1.83	0.06	4.41	1.04
RMSE (mm)	20.37	113.62	42.76	7.56	66.39	32.19

Table 4 presents the MSE and RMSE of the estimated PD locations based on the TDOAs from the FPM. Based on the MSE, the estimated PD locations in RBDPO have lower errors than in MO across all x-, y-, and z-axes. The x-axis records the lowest MSE at 0.06 mm^2. The RMSE displays a similar trend to the MSE, whereby the PD localisation in RBDPO yields lower errors in the x- and z-axes, at 7.56 mm and 32.19 mm as compared to MO. For the y-axis, RBDPO records an RMSE of 66.39 mm, which is the highest among the 3 axes but still 47.23 mm lower than in MO.

The MSE and RMSE of the estimated PD locations that are computed with the TDOAs from the CEM are reported in Table 5. For MO, the highest MSE and RMSE among the 3 axes occur along the y-axis, at 15.98 mm^2 and 126.43 mm, respectively. A similar pattern is observed in RBDPO, where the y-axis also records the largest errors, with an MSE of

Table 5
MSE and RMSE of PD localisation based on TDOAs from the CEM

	MO			RBDPO		
	X	Y	Z	X	Y	Z
MSE (mm^2)	0.32	15.98	1.78	0.55	32.05	7.17
RMSE (mm)	17.99	126.43	42.32	23.52	179.03	84.10

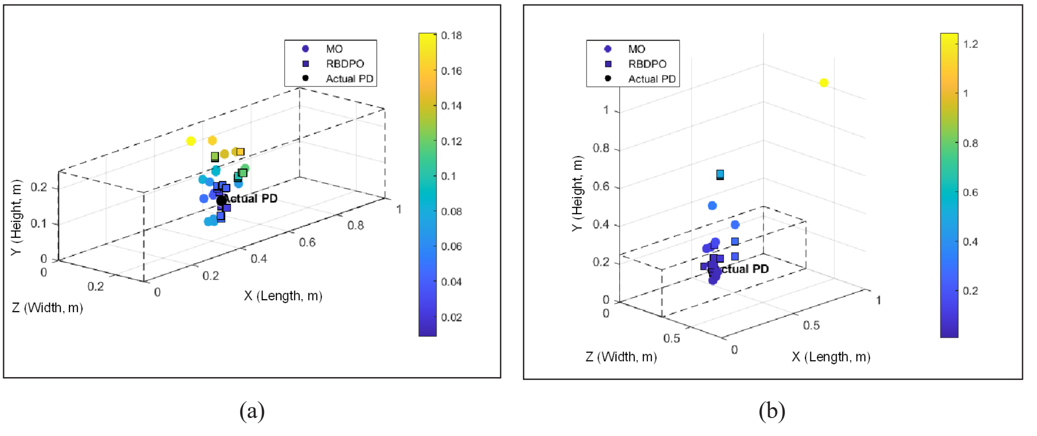

Figure 9. 3D heatmap scatter plot of the LE of the estimated PD locations in MO and RBDPO based on TDOAs obtained through (a) FPM and (b) CEM

32.05 mm^2 and RMSE of 179.03 mm. According to these analyses, the PD localisation in RBDPO based on the TDOAs from the FPM produces the lowest MSE and RMSE among all cases, regardless of the axis. These results align with the LE and RE analyses, which showcase that the TDOAs from the FPM generally lead to higher localisation accuracy, and that for the FPM, PD localisation in RBDPO is better than in MO.

The 3D heatmap scatter plot of the LE of the estimated PD locations in MO and RBDPO is illustrated in Figure 9. Figure 9(a) and Figure 9(b) present the estimated PD locations computed from the TDOAs of the FPM and CEM, respectively. The actual PD location is shown as a black marker, while the estimated PD locations in MO and RBDPO are represented by circular and square markers, respectively. The colour gradient indicates the magnitude of LE, whereby blue to green colours represent lower LE values, while yellow colours represent higher LE values. Figure 9(a) clearly highlights the contrast in localisation accuracy between the oil samples. The RBDPO cluster appears tight around the actual PD location without any yellow square markers, and the LEs remain below 0.18 m. For PD localisation based on the TDOAs from the CEM, the LEs are larger as compared to those from the FPM. This is evident in Figure 9(b), where the colour scale exceeds 1 m, and several estimated PD locations fall outside the tank. This result is consistent with the LE and RE results in Figure 8.

CONCLUSION

This study presented an experimental comparison of PD localisation performance in MO and RBDPO based on the UHF method. The UHF PD signals are recorded experimentally, while electrical PD signals are acquired in parallel to confirm the occurrence of PDs. It is found that RBDPO achieves lower LE and RE as compared to MO based on the TDOAs obtained from the FPM. Conversely, CEM produces significantly larger errors than FPM for PD localisation in both MO and RBDPO. Furthermore, the 3D heatmap scatter plots demonstrate that the estimated PD locations in RBDPO are clustered closely around the actual PD source, whereas those in MO exhibit slightly broader dispersion. Overall, UHF PD detection and localisation in RBDPO are experimentally demonstrated to be feasible. These findings support the potential application of natural esters such as RBDPO as alternative insulation in transformers, where the insulation condition can be effectively monitored through the UHF method.

ACKNOWLEDGEMENT

This research was funded by Universiti Putra Malaysia, Putra Grant Scheme, Inisiatif Putra (GP- FASTRACK/2024/9791100) and (GP-IPI (KMD)/2023/9756300).

LIST OF ABBREVIATIONS

PD	:	Partial discharge
RBDPO	:	Refined, Bleached and Deodorised Palm Olein
MO	:	Mineral Oil
UHF	:	Ultra-High Frequency
TOA	:	Time of Arrival
TDOA	:	Time Difference of Arrival
FPM	:	First Peak Method
CE	:	Cumulative Energy
CEM	:	Cumulative Energy Method
IMC:	:	Impedance Matching Circuit
MSE	:	Mean Squared Error
RMSE	:	Root Mean Squared Error
LE	:	Localisation Error
RE	:	Relative error

REFERENCES

Adak, S., & Cangi, H. (2024). The quality problems at low irradiance in the grid-connected photovoltaic systems. *Electrical Engineering, 106*(5), 6185-6197.https://doi.org/10.1007/s00202-024-02351-6

Ahmad, N. D., Azis, N., Jasni, J., & Rezali, K. A. (2025). Acoustic partial discharge localisation in refined, bleached and deodorised palm oil (RBDPO) based on the Savitzky-Golay and moving average denoising methods. *Pertanika Journal of Science & Technology, 33*, 115-128. https://doi.org/10.47836/pjst.33.S4.07

Ahmad, N. D., Hashim, A. H. M., Azis, N., Talib, M. A., Rezali, K. A. M., Nik Ali, N. H., Jasni, J., Masahiro, K., & Jamil, M. K. M. (2023). Partial discharge localisation of refined bleached deodorised palm oil (RBDPO) based on the acoustic emission method. *APL 2023- 12th Asia-Pacific International Conference on Lightning*, 1-5. https://doi.org/10.1109/APL57308.2023.10181667

Antony, D., Mishra, P., Todi, A., John, N. A., & Patankar, A. M. (2021). Partial discharge localisation in transformers using UHF technique: Non-iterative method. *International Journal of Information Technology, 13*(1), 291-297.https://doi.org/10.1007/s41870-020-00481-1

Azis, N., Jasni, J., Ab Kadir, M. Z. A., & Mohtar, M. N. (2014). Suitability of palm-based oil as a dielectric insulating fluid in transformers. *Journal of Electrical Engineering & Technology, 9*(2), 662-669.https://doi.org/10.5370/JEET.2014.9.2.662

Azmi, K., Zuhairi, A., Ishak, D., Muhamad, N. A., & Kamarol, M. (2017). Partial discharge characteristics of spherical metal particles in mineral oil and PFAE under AC voltage. In *Proceedings of the 2017 IEEE Region 10 Conference (TENCON)* (pp. 2588-2593). https://doi.org/10.1109/TENCON.2017.8228298

Chai, H., Lu, S., Phung, B. T., & Mitchell, S. (2019). Comparative study of partial discharge localisation based on UHF. In *Proceedings of the 25th International Conference on Electricity Distribution* (pp. 3-6).

Chan, J. Q., Raymond, W. J. K., Illias, H. A., & Othman, M. (2023). Partial discharge localisation techniques: A review of recent progress. *Energies, 16*(6). https://doi.org/10.3390/en16062863

Chandrasekar, S., & Montanari, G. C. (2014). Analysis of partial discharge characteristics of natural esters as dielectric fluid for electric power apparatus applications. *IEEE Transactions on Dielectrics and Electrical Insulation, 21*(3), 1251-1259. https://doi.org/10.1109/TDEI.2014.6832272

Desai, B. M. A., & Sarathi, R. (2018). Identification and localisation of incipient discharges in transformer insulation adopting UHF technique. *IEEE Transactions on Dielectrics and Electrical Insulation, 25*(5), 1924-1931.https://doi.org/10.1109/TDEI.2018.007294

Dombek, G., & Gielniak, J. (2023). Dielectric properties and fire safety of mineral oil and low-viscosity natural ester mixtures in various concentrations. *Energies, 16*(10). https://doi.org/10.3390/en16104195

Durga, G., Mahidhar, P., Karthikeyan, A. S., Sarathi, R., Taylor, N., & Edin, H. (2020). *Dielectric properties of mixed mineral and synthetic ester oil*. https://doi.org/10.1049/iet-smt.2019.0227

Gautam, L., Sarathi, R., Soundarya, P., Sekar, G., Rao, U. M., & Fofana, I. (2023). Understanding the surface discharge characteristics of thermally aged ester fluid impregnated pressboard adopting the fluorescent fibre technique. *Proceedings of the International Symposium on Electrical Insulating Materials*, 211-214. https://doi.org/10.23919/ISEIM60444.2023.10329150

Gautam, L., Sarathi, R., Soundarya, P., Sekar, G., Rao, U. M., & Fofana, I. (2024). Quantitative estimation of the gelling in thermally aged natural ester dielectric liquid. *IEEE Transactions on Dielectrics and Electrical Insulation, 31*(2), 897-903. https://doi.org/10.1109/TDEI.2023.3340632

Girish, S. K., Sumangala, B. V., Raviprasad, D., & Jagadisha, K. R. (2021). Investigations on partial discharge characteristics of vegetable oil and mineral oil. *International Journal of Engineering Research & Technology (IJERT), 10*(2), 95-97.

Ha, S. G., Cho, J., Lee, J., Min, B. W., Choi, J., & Jung, K. Y. (2018). Numerical study of estimating the arrival time of UHF signals for partial discharge localisation in a power transformer. *Journal of Electromagnetic Engineering and Science, 18*(2), 94-100. https://doi.org/10.26866/jees.2018.18.2.94

HadiAlnashia, I. A., Ibrahim Mohd, I., Almelian, M. M., & Omran, M. A. (2018). The impact of partial discharge on the dielectric properties of refined bleached and deodorised palm oil (RBDPO). *Journal of Telecommunication, Electronic and Computer Engineering, 10*(1-3), 81-85.

Jangjoo, M. A., Allahbakhshi, M., & Mirzaei, H. R. (2023). UHF sensors positioning on the power transformer tank to enhance the partial discharge localisation accuracy. *Electric Power Systems Research, 218*, Article 109174. https://doi.org/10.1016/j.epsr.2023.109174

Jaroszewski, M., & Rakowiecki, K. (2017). Partial discharge inception voltage in transformer natural ester liquid -Effect of the measurement method in the presence of moisture. *IEEE Transactions on Dielectrics and Electrical Insulation, 24*(4), 2477-2482. https://doi.org/10.1109/TDEI.2017.005917

Khelifa, H., Skotnicki, P., Beroual, A., Vagnon, E., & Jaroszewski, M. (2024). Effect of MgO nanoparticles on the AC breakdown voltage, partial discharge activity, and electrostatic charging tendency of natural ester. *IEEE Transactions on Dielectrics and Electrical Insulation, 31*(3), 1350-1358. https://doi.org/10.1109/TDEI.2024.3374244

Kurimský, J., Rajňák, M., Šárpataky, M., Čonka, Z., & Paulovičová, K. (2021). Electrical and acoustic investigation of partial discharges into two types of nanofluids. *Journal of Molecular Liquids, 341*, Article 117444. https://doi.org/10.1016/j.molliq.2021.117444

Lam, K. Y. (2024). *Dissolved gas analysis (DGA) for natural ester-filled transformers*. Cargill Brand.

Mengounou, G. M., Jiosseu, J. L., & Imano, A. M. (2022). Experimental investigation of partial discharge activities in palm kernel oil methyl ester and mineral oil by using a Rogowski coil. *Electric Power Systems Research, 213*, Article 108708. https://doi.org/10.1016/j.epsr.2022.108708

Mina-Casaran, J. D., García, B., García, D. F., Gómez, A. M., & Montero, A. (2025). Partial discharge patterns in natural esters from different vegetable bases. *IEEE Transactions on Dielectrics and Electrical Insulation, 32*(1), 435-443. https://doi.org/10.1109/TDEI.2024.3486275

Mohamad, N. A., Azis, N., Jasni, J., Ab Kadir, M. Z. A., Yunus, R., Ishak, M. T., & Yaakub, Z. (2014). A study on the dielectric properties of palm oil and coconut oil. In *2014 IEEE International Conference on Power and Energy (PECon)* (pp. 109-112). IEEE. https://doi.org/10.1109/PECON.2014.7062423

Mohamad, N. A., Azis, N., Jasni, J., Kadir, M. Z. A., Yunus, R., & Yaakub, Z. (2018). Physiochemical and electrical properties of refined, bleached and deodorised palm oil under high temperature ageing for application in transformers. *Energies, 11*(6). https://doi.org/10.3390/en11061583

Mohamad, N. A., Azis, N., Jasni, J., Mohd Zainal, M. Z. A., Yunus, R., & Yaakub, Z. (2021). Experimental study on the partial discharge characteristics of palm oil and coconut oil-based Al2O3 nanofluids in the presence of sodium dodecyl sulfate. *Nanomaterials, 11*(3), 1-18. https://doi.org/10.3390/nano11030786

Mohan Rao, U., Fofana, I., Jaya, T., Rodriguez-Celis, E. M., Jalbert, J., & Picher, P. (2019). Alternative dielectric fluids for transformer insulation system: Progress, challenges, and prospects. *IEEE Access, 7*, 184552-184571. https://doi.org/10.1109/ACCESS.2019.2960020

Mohd Hashim, A. H., Azis, N., Jasni, J., Mohd Radzi, M. A., Kozako, M., Kamarol Mohd Jamil, M., & Yaakub, Z. (2022). Partial discharge localisation in oil through acoustic emission technique utilising fuzzy logic. *IEEE Transactions on Dielectrics and Electrical Insulation, 29*(2), 623-630. https://doi.org/10.1109/TDEI.2022.3157911

Mu, G., Dai, Q., Chai, S., & Yang, P. (2024). Ultrasonic propagation characteristics of partial discharge in oil-impregnated paper traction transformers. *AIP Advances, 14*(3). https://doi.org/10.1063/5.0191688

Muangpratoom, P., Suriyasakulpong, C., Maneerot, S., Vittayakorn, W., & Pattanadech, N. (2023). Experimental study of the electrical and physicochemical properties of different types of crude palm oils as dielectric insulating fluids in transformers. *Sustainability, 15*(19), Article 14269. https://doi.org/10.3390/su151914269

Murad, T. K., Syakur, A., & Setiawan, I. (2025). Analysis of partial discharge characteristics in transformer oil insulation media using needle-plane and plane-plane electrode systems. *International Journal of Electrical and Computer Engineering (IJECE), 15*(5), 4445-4453. https://doi.org/10.11591/ijece.v15i5.pp4445-4453

Perfetto, L., & D'Antona, G. (2021). Experimental results of partial discharge localisation in bounded domains. *Sensors, 21*(3), Article 935. https://doi.org/10.3390/s21030935

Qian, S., Chen, H., Xu, Y., & Su, L. (2018). High sensitivity detection of partial discharge acoustic emission within power transformers by Sagnac fibre optic sensor. *IEEE Transactions on Dielectrics and Electrical Insulation, 25*(6), 2313-2320. https://doi.org/10.1109/TDEI.2018.007131

Rajab, A., Ardison, A., Pratama, R. W., Novendra, R., Baharuddin, B., & Artono, T. (2025). Dissolved gas analysis of methyl ester-mineral oil mixture under partial discharge. *TEM Journal, 14*(1), 55-63. https://doi.org/10.18421/TEM141-06

Rathod, V. B., Kumbhar, G. B., & Bhalja, B. R. (2021). Partial discharge detection and localisation in power transformers based on acoustic emission: Theory, methods, and recent trends. *IETE Technical Review, 39*(3), 540-552. https://doi.org/10.1080/02564602.2021.1873155

Sinaga, H. H., Phung, B. T., & Blackburn, T. R. (2011). Partial discharge localisation in transformers using UHF sensors. *Electrical Insulation Conference*. https://doi.org/10.1109/EIC.2011.5996117

Sinaga, H. H., Phung, B. T., & Blackburn, T. R. (2012). Partial discharge localisation in transformers using UHF detection method. *IEEE Transactions on Dielectrics and Electrical Insulation, 19*(6), 1891-1900. https://doi.org/10.1109/TDEI.2012.6396945

Song, L. (2004). *Detection and position location of partial discharges in transformers using fibre optic sensors* [Thesis]. Virginia Tech. http://scholar.lib.vt.edu/theses/available/etd-12032004-151222/

Suhaimi, N. S., Zainul Ariffin, K. N., Zaini, N. H., Abdul Rahman, S., Azizan, M. M., & Rameli, N. (2025). Palm oil as a transformer insulating fluid: A review. *Semarak Proceedings of Natural and Environmental Sciences, 3*(1), 13-17. https://doi.org/10.37934/spnes.3.1.1317a

Thiviyanathan, V. A., Ker, P. J., Leong, Y. S., Abdullah, F., Ismail, A., & Zaini Jamaludin, M. (2022). Power transformer insulation system: A review of the reactions, fault detection, challenges and prospects. *Alexandria Engineering Journal, 61*(10), 7697-7713. https://doi.org/10.1016/j.aej.2022.01.026

Uwiringiyimana, J. P., Khayam, U., Montanari, G. C., & Hikita, M. (2022). Comparative analysis of partial discharge detection features using a UHF antenna and conventional HFCT sensor. *IEEE Access, 10*, 107214-107226. https://doi.org/10.1109/ACCESS.2022.3212746

Working Group D1.33. (2012). *High-voltage on-site testing with partial discharge measurement*. CIGRE Publication.

Wu, H., Liu, H., Xue, Z., Yang, J., Li, Q., He, D., & Siew, W. H. (2022). The generation and migration of bubbles in oil-pressboard insulation. *IEEE Transactions on Dielectrics and Electrical Insulation, 29*(6), 2110-2121. https://doi.org/10.1109/TDEI.2022.3210486

Xavier, G. V. R., de Oliveira, A. C., Silva, A. D. C., Nóbrega, L. A. M. M., da Costa, E. G., & Serres, A. J. R. (2021). Application of time difference of arrival methods in the localisation of partial discharge sources detected using bio-inspired UHF sensors. *IEEE Sensors Journal, 21*(2), 1947-1956. https://doi.org/10.1109/JSEN.2020.3019760

Yu, R., & Zhang, Z. (2024). Transformer partial discharge location technology based on gradient oil temperature. *Frontiers in Energy Research, 12*, 142801. https://doi.org/10.3389/fenrg.2024.1428012